Ionization and fragmentation of C_{60} in charge-transfer collisions of 2-MeV lithium ions

A. Itoh, H. Tsuchida,* T. Majima, and N. Imanishi
Department of Nuclear Engineering, Kyoto University, Kyoto 606-8501, Japan
(Received 7 December 1998)

Collision-induced ionization and fragmentation of C_{60} molecules are studied using 2-MeV Li^{q+} projectile ions with $q=1-3$. Cross sections for the production of fragment ions C_n^+ $(n=1-14)$ and ionized parent ions C_{60}^{r+} $(r=1-4)$ were obtained by time-of-flight measurements in coincidence with outgoing projectiles with charge states k ranging from 0 to 3. The mass-to-charge spectra revealed a wide variety of distribution patterns for different $q\rightarrow k$ collision processes. For all three incident charges, the degree of target ionization and fragmentation was found to increase with increasing number of electrons captured by or lost from the projectile ions in collisions. Analysis of cross section data for small fragment ions provides evidence of the quasiequilibrium charge distribution achieved for ions penetrating the C_{60} molecular cage. [S1050-2947(99)07106-1]

PACS number(s): 34.70.+e, 36.40.−c

I. INTRODUCTION

In the past few years the study of fragmentation and ionization processes of C_{60} molecules has become a subject of increasing interest due to its fundamental and practical importance in many areas of physics, chemistry, astrophysics, and materials science [1]. In particular a great deal of information has been accumulated in experiments using photoabsorption and electron-impact methods about various electronic properties such as ionization potentials and the appearance energies of various fragment ions, the giant resonance connected with plasmon excitation, the electron energy loss function, and so forth [2–16]. The fragmentation mechanism of C_{60} has been studied using mainly accelerated fullerene ions in collisions with various gaseous targets [17–20] in the energy range below several keV in the center-of-mass system. Among these experimental investigations Campbell, Raz, and Levine [20] studied also theoretically and pointed out that the distribution pattern of fragment ions is closely related to the internal energy of C_{60}. For instance, they demonstrated that an internal energy above 225 eV (~4000 K) leads to the breakdown of the molecule into entirely small fragment ions (multifragmentation).

Contrary to the wealth of investigations above, only a few experimental studies have been carried out for the collision-induced fragmentation process by energetic ion impact [21–30]. In these collisions several different inelastic collisions may take place simultaneously, revealing many-body properties such as collective excitation, multiple ionization, electron capture and loss, Auger processes following inner-shell ionization, direct knockoff of constituent atoms, and so forth. Consequently, the situation becomes greatly complicated and the mechanism leading to, for instance, multifragmentation of C_{60} is not yet known precisely. In order to achieve a detailed understanding it is necessary to know the separate contributions from each inelastic process. Pioneering work of such experiments was done by Walch *et al.* [21] using highly charged, slow Ar^{8+} ions. They measured fragment ions in coincidence with outgoing projectile charge states formed via capture of one through eight electrons from the C_{60} target. They showed that multiple-electron capture induces multifragmentation of C_{60}, while a few-electron capture leads only to the formation of intact C_{60}^{r+} ions. A similar but more detailed experimental study on the relationship between small fragment ions C_n^+ and incident charge states has been done recently by Schlathölter, Hoekstra, and Morgenstern using slow O^{1+-7+} ions [28]. The formation process of large daughter ions $C_{60-2m}^{r'+}$ from multiply charged C_{60}^{r+} ions was investigated by Martin *et al.* [29] for slow Xe^{8+} ions by triple coincidence measurements including also the number of ejected electrons. On the other hand, little experimental work of this kind has been reported for collisions of fast projectile ions. Nakai *et al.* [27] performed measurements in coincidence with outgoing projectile charge states using 15.6-MeV carbon ions ($v=7.2$ a.u.). They obtained fragment ion spectra exhibiting only small fragments of $n\leqslant 10$ even for the single-electron-loss and -capture processes of $C^{5+,6+}$ projectiles in close collisions with the target. Their result indicates clearly that the impact parameter between the incident ion and the target plays also an important role in the multifragmentation process in fast-ion–C_{60} collisions.

In this work we study the fragmentation and ionization process of C_{60} in collisions with 2-MeV Li^{1+-3+} ions ($v=3.38$ a.u.). Fragment ions and ionized parent ions produced in charge-transfer collisions were measured in coincidence with outgoing projectile charge states. The measurement was extended to include the process without changing the charge state before and after collisions. This process will be referred to as a ''direct process'' herein-after. The measurement was also carried out using a beam chopping technique [26] to obtain, with good accuracy, the total production cross sections corresponding to the sum over all outgoing charge states.

This paper is organized as follows. In Sec. II the experimental arrangement and the procedure to determine cross sections are described in detail. In Sec. III we first discuss the characteristic features extracted from time-of-flight (TOF) spectra measured in various charge-transfer processes.

*Present address: Department of Physics, Nara Women's University, Nara 630-8506, Japan.

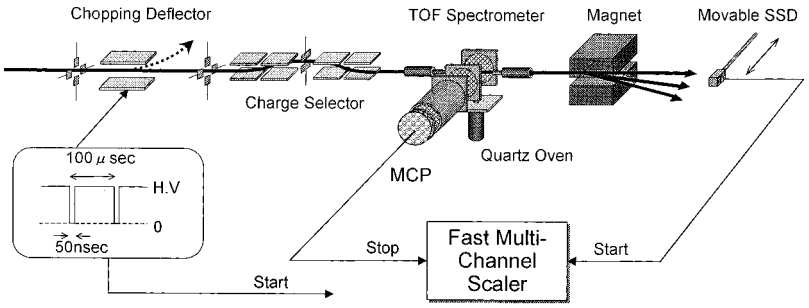

FIG. 1. Schematic sketch of the experimental arrangement.

Then we discuss ionization and fragmentation using cross-section data. Ionization cross sections of C_{60} are compared with those reported previously in ion-atom collisions. Fragmentation is discussed in relation to energy deposition from the projectile to the target molecule. Finally, we present evidence of the quasiequilibrium charge-state distribution in outgoing particles penetrating the molecular cage. Concluding remarks are given in Sec. IV.

II. EXPERIMENT

The experiment was performed at the 1.7-MV tandem Cockcroft-Walton accelerator facility of Kyoto University. Figure 1 shows a schematic diagram of the experimental setup. A beam of 2-MeV Li^{q+} ions ($q=1-3$) from the accelerator was collimated to a diameter smaller than 1 mm with two sets of four-jaw slits. To remove impurity ions of undesirable charge states the incident beam was led to a charge-selection chamber consisting of four electrostatic deflectors, as shown in Fig. 1. The charge-selected beam then entered a crossed-beam collision chamber where the ions interacted with a gas-phase C_{60} target. To achieve differential pumping two cylindrical slits (5 mm in diameter and 3 cm in length) were set at the entrance and the exit of the collision chamber. Outgoing projectiles were then charge separated by a magnet and detected by a movable solid-state detector (SSD). The base pressure was about 3×10^{-7} Torr both in the beam line and in the collision chamber.

The mass-to-charge distribution of fragment ions produced in collisions between projectiles and C_{60} was measured with a TOF spectrometer located at a right angle to the incident beam. As described in [26], the TOF spectrometer consists of an extraction region (4 cm), an acceleration region (1.5 cm), and a drift region (16.2 cm) in conjunction with a two-stage multichannel plate (MCP) detector (4 cm in diameter). Extraction of fragment ions was made by placing ±750 V on two Mo-mesh grids separated by 4 cm so as to keep the beam axis at the Earth's potential. The size of these grids was 6 and 5 cm in the horizontal (beam axis) and vertical directions, respectively. The spectrometer was operated under a Wiley-McLaren spatial-focusing condition [31]. The TOF spectra of fragment ions were obtained using a fast-multichannel scaler (FMCS, LN-6500, Labo.) with the highest time resolution of 1 ns enabling us to detect multiple ions of different mass to charge produced in a single collision event. In the present experiment the FMCS was operated with the time resolution of 8 ns/channel in 2048 total channels. A flight time of the slowest C_{60}^{+} ions was about 12 μs. Note that the detection efficiency due to ion multiplicity is not considered in this experiment.

Using two different start pulses in TOF measurements, we obtained the total and partial distributions of the fragment ions separately. First, the total distribution measurement was performed by chopping the incident beam with 10 kHz and about 50 ns width by an electrostatic beam chopping system as shown in Fig. 1. The start pulse to the FMCS was generated by the chopping control system. Second, the partial distributions were obtained by coincidence measurements between fragment ions and outgoing projectile charge states. This was achieved with start trigger pulses from SSD signals of the particles with the desired charge states.

The peak intensity Y of the fragment ions is related to the production cross section σ in the form $Y=\sigma I_0 XTGFO$, where I_0 is the incident beam flux, X the effective target thickness (a product of a target density and an effective target length), T the collection efficiency of the TOF spectrometer, G the total transmission of grids (0.55), F the relative detection efficiency of the MCP, and O the MCP open area ratio (0.57).

A C_{60} target was produced by heating a C_{60} powder of 99.98% purity at 465 °C in a temperature-controlled quartz oven located at the base of the chamber. An effusive C_{60} beam was introduced upward into a collision region through a hole (2 mm in diameter) opened at the top of the oven. The beam axis of incident lithium ions was about 37 mm high from the hole. Under this geometrical condition the effusion of C_{60} molecules into the collision region can be considered to follow Knudsen's cosine law, resulting in a rather broad density distribution $n(x)$ along the beam axis, as demonstrated in Fig. 2. In this figure a position on the beam axis right above the hole of the oven is taken as the origin of the abscissa and x is the distance from this point along the beam axis. Absolute values of the target density were determined from the vapor pressure data reported by Abrefah *et al.* [32]. The estimated value of $n(0)$ was 1.9×10^{10} (molecules/cm^3), which is equivalent to 4.9×10^{-7} Torr, with their vapor pressure of 2.2×10^{-4} Torr inside the oven at 465 °C.

The collection efficiency T representing an ion-arrival efficiency at the MCP front plate depends on the initial kinetic energy (ε) and the emission position (x) of the ions. From the ray-trace simulation described in [26], the collection efficiency $T(x)$ was calculated for various values of ε with an assumption of isotropic emission in 4π directions. Several examples of the results are demonstrated in Fig. 2. Near the position corresponding to the edge of the MCP one can see ''escape'' from the MCP area and ''flow in'' from outside the area; such an effect becomes significant with increasing ε, as expected. The TOF peak profile analysis [26] using these $T(x)$ gives information about the initial energy distri-

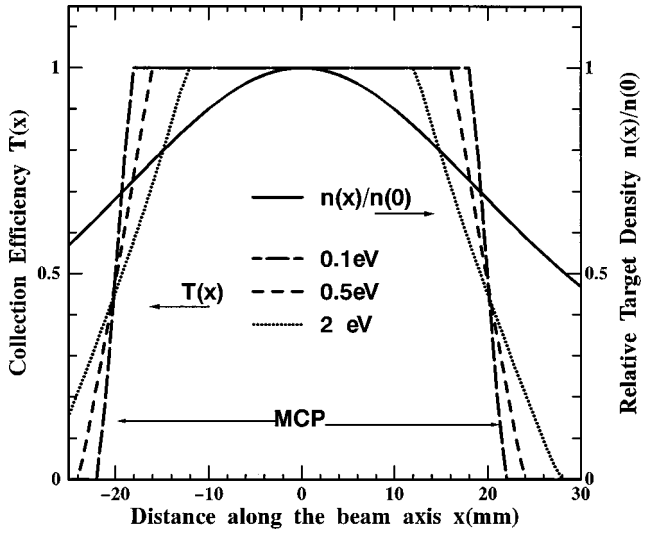

FIG. 2. Distribution of C_{60} target number density $n(x)$ divided by $n(0)$ along the beam axis and ion-collection efficiency $T(x)$ for various initial energies as denoted.

bution of fragment ions. It was found that the mean energies were 1–2 eV for small fragment ions C_n^+ ($n \leqslant 12$) and less than 0.1 eV for parent ions C_{60}^{r+}. The actual value of the effective target thickness X is determined by integrating a product $n(x)T(x)$ over x; it varies depending on ε. Calculated values of X for $\varepsilon = 0$, 0.1, 0.5, and 2 eV were 0.878, 0.878, 0.873, and 0.851 in units of $n(0)L$ with $L = 4$ cm, the MCP detection size. Consequently, we can approximate X to be about 6.6×10^{10} (molecules/cm^2).

The detection efficiency F of the MCP for various fragment ions was determined from measurements of intensity variation of fragment ions as a function of impinging energy on the MCP front plate. This was achieved by changing the voltage V placed on the front plate in the range from -2 to -5 kV, giving rise to the impinging energies of 2–20 keV for, e.g., C_{60}^{1+-4+} ions. The results obtained for C_{60}^{r+} are shown in Fig. 3. By fitting a smooth curve to a set of data,

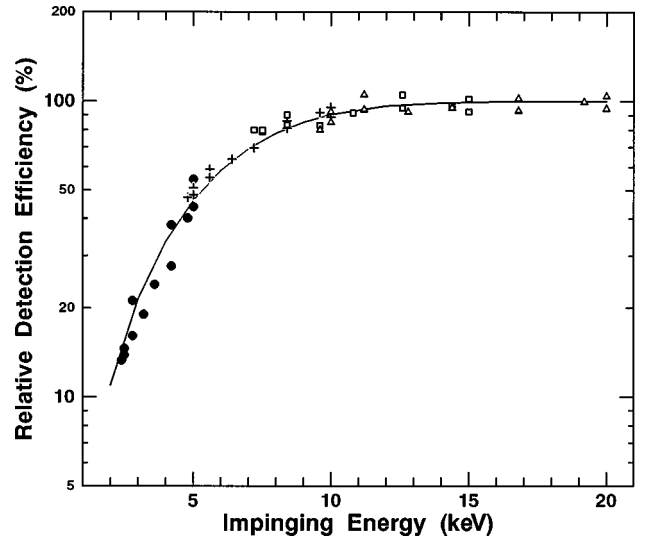

FIG. 3. Relative detection efficiency of the MCP for C_{60}^{r+} ions as a function of impinging energy: ●, C_{60}^+; +, C_{60}^{2+}; □, C_{60}^{3+}; △, C_{60}^{4+}.

the efficiency F at the impinging energy E(keV) was determined to be $-100\ln(1-F) = 1.48E + 2.18E^2$. Here a plateau part observed at higher energies was taken to be unity. The front voltage used in the present work was -4 kV, giving rise to an F of 0.34, 0.78, 0.96, and 1 for $q = 1$, 2, 3, and 4, respectively. On the other hand, the intensity change was not observed within statistical errors for small fragment ions C_n^+ ($n \leqslant 14$), indicating $F \simeq 1$ for these ions. Note that the present F values given by the above formula are very close to those reported in [21].

Since the velocity (7.3×10^8 cm/s) of 2-MeV Li^{q+} ions is fast enough to exclude negative-ion formation in collisions, the peak intensity observed by the chopping mode may always be the sum of partial intensities from four charge-transfer processes $q \rightarrow k$ including a direct process $q \rightarrow q$. The peak intensities of an fth fragment ion measured by the chopping mode and by the charge-changing mode can be expressed, respectively, by

$$Y_f(C) = I_0(C)X\sigma_f(C) = I_0(C)X\sum_{k=0}^{3}\sigma_f(qk), \qquad (1)$$

$$Y_f(qk) = I_0(qk)X\sigma_f(qk) = \frac{I_{qk}(S)}{\Phi_{qk}}X\sigma_f(qk), \qquad (2)$$

where C and qk represent, respectively, the chopping mode and the charge-changing mode ($q \rightarrow k$), $I_{qk}(S)$ is the number of outgoing particles with charge k detected by the SSD, and Φ_{qk} is the charge fraction of outgoing projectiles with charge k. To avoid confusion the peak intensities given above represent corrected values with respect to *GFO*. It is obvious that the $Y_f(C)$ is simply a sum of four $Y_f(qk)$ if the incident flux is the same for both modes. The total number of ions detected by the MCP, irrespective of coincidence or noncoincidence events, was used as a monitor of the incident beam flux, which was varied appropriately for each measurement because of limited count-rate efficiency of the SSD. This monitoring method enables us to determine total cross sections $\sigma_f(C)$ in the chopping mode measurements. The production cross sections $\sigma_f(qk)$ were determined from Eq. (2) using charge fractions measured by moving the SSD within a range covering all charge states. In direct processes $q \rightarrow q$ it was often hard to achieve good counting statistics because nearly all ions detected by the SSD are the particles that underwent no interactions with the target. Thus the cross sections $\sigma_f(qq)$ for the direct processes were cross-checked using the relation (1) between the cross sections $\sigma_f(C)$ and $\sigma_f(qq)$. Note that the measured charge fractions Φ_{qk} include also contributions from charge-transfer collisions with residual gases occurring inside and outside the observation region up to the entrance part of the charge separation magnet.

Finally, it should be noted that the vapor pressure data are substantially scattered throughout the literature [32–34]. For instance, at 465 °C, they are 1.6×10^{-4} [33], 5.5×10^{-4} [34], and 3.2×10^{-4} Torr [34]. Therefore, the systematic error of the present experiment is supposed to be a factor of 2, while the overall relative errors arising from other factors were estimated to be 20–30 %.

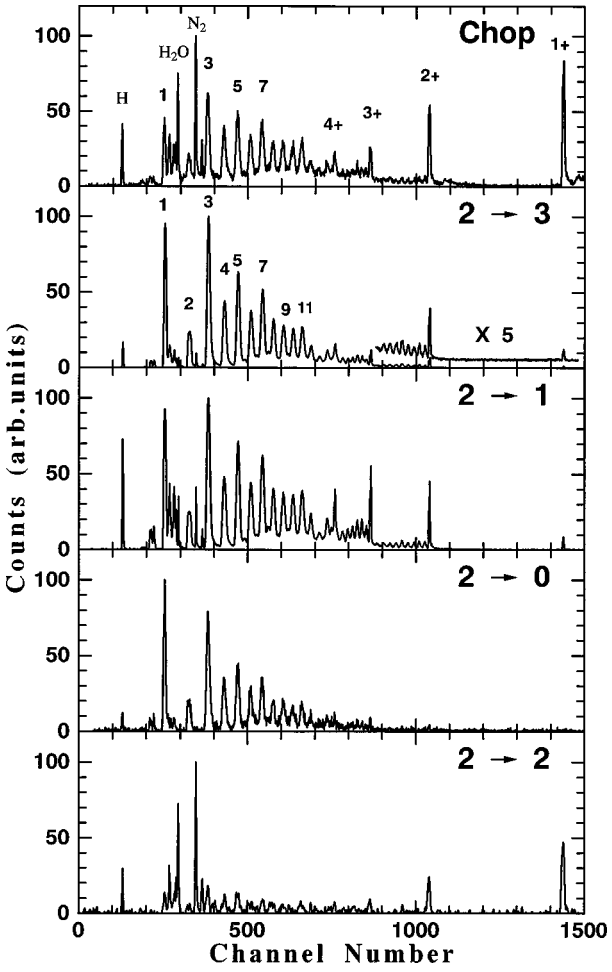

FIG. 4. TOF spectra obtained for 2-MeV Li^{2+} on a C_{60} target. The number represents the charge-transfer process $2 \rightarrow k$ and the uppermost spectrum corresponding to the total distribution was obtained by the chopping mode.

III. RESULTS AND DISCUSSION

A. TOF spectra

Figure 4 shows examples of total and partial distributions of TOF spectra obtained, respectively, by the chopping mode and the charge-changing mode, where the incident beam is 2-MeV Li^{2+} ions. In the total spectra depicted in the uppermost figure one can see prominent peaks originating from ionized parent ions C_{60}^{r+} (up to $r=4$), small fragment ions C_n^+ with n ranging from 1 to 14, and residual impurity gases. Note that the C_{60}^{4+} and C_{15}^+ ions are observed at the same TOF position. The peak intensity of C_{60}^{r+} decreases with increasing degree of ionization r. Large daughter ions C_{60-2m}^{r+}, produced via evaporation of even-numbered carbon atoms [14,29], are found to be weak. The intensities of these ions relative to their parent ions increase with increasing r, indicating that the internal energy in ionization processes increases also with r. An even-odd oscillation of peak intensities is observed in small fragment ions. The overall features mentioned above are essentially the same as in previous experiments using the pulsed beam method [22,26,27].

Dramatic changes in relative intensities are observed in the spectra by the charge-changing mode. For the single-electron-loss process $(2 \rightarrow 3)$, the intensities of the intact C_{60}^{r+} ions decrease substantially in comparison to small fragment ions. Moreover, the intensity reverse between C_{60}^+ and C_{60}^{2+} is observed clearly. In small fragments one can see a rather large enhancement of lighter fragment ions, in particular C^+ ions, in comparison to heavier ones $(n \geq 4)$, while the relative intensities of these heavier fragment ions do not change significantly from those observed by the chopping mode.

In single-electron-capture collisions $(2 \rightarrow 1)$, doubly and multiply ionized parent ions are produced rather strongly with peak intensities of the same order of magnitude as the small fragment ions. The result indicates that the multiple ionization is preferred even in the single-capture process. The distribution pattern of small fragment ions is similar to the spectra in $2 \rightarrow 3$ processes, although the enhancement of $C_{1,3}^+$ ions is not as strong as in $2 \rightarrow 3$ processes.

The substantially different spectral pattern is obtained for the double-electron-capture process $(2 \rightarrow 0)$. Here the peak intensities of the parent ions are considerably reduced compared to the fragmentation part. In particular, the C_{60}^+ ion was not observed within statistical errors, which was ensured by repeating the measurements a few times, supporting the single-collision condition. Also, electron capture by slow C_{60}^{2+} ions during flight inside the TOF spectrometer can be neglected. In fact, the mean free path $\sim (n_b \sigma)^{-1}$ for capture collisions by ions with energies ~ 1 keV is roughly 900 m, corresponding to a capture time of about 50 ms with $\sigma \sim 10^{-15}\,\mathrm{cm}^2$ at the background pressure 3×10^{-7} Torr. This capture time is much longer than the C_{60}^{2+} flight time of 8.5 μs. The experimental evidence of substantially weak C_{60}^{r+} ions in comparison to small fragment ions implies that the double-capture collision is essentially different from the rather gentle double-capture processes observed in highly charged slow ion impacts [21] where the most intensive peaks are C_{60}^{r+} and no small fragment ions were produced. Thus we conclude that the double-capture collisions by fast ions induces predominantly the target fragmentation rather than forming ionized parent ions. This characteristic is also the case for the $2 \rightarrow 3$ process, as seen in Fig. 4. The intensity distribution of small fragment ions is similar, but reveals a large enhancement of C^+ ions in comparison to the case of the $2 \rightarrow 3$ process.

The spectrum obtained for collisions accompanying no charge change $(2 \rightarrow 2)$ is shown in the bottom figure. Bad counting statistics is due to the reason given in Sec. II. The spectrum obtained is apparently similar to the total distribution (chopping mode) particularly for the intensity distribution of C_{60}^{r+} ions in the ionization part. This implies that the total distribution is dominated by the $2 \rightarrow 2$ direct process.

Fragment ion spectra obtained for other incident charge states ($q=1$ and 3) are shown in Fig. 5. Characteristic features are discussed briefly. For Li^+ incidence, single-electron-loss $(1 \rightarrow 2)$ and single-electron-capture $(1 \rightarrow 0)$ processes were found to produce distribution patterns similar to each other and the ionization part was rather strongly enhanced in both cases. This is greatly different from Li^{2+} incidence, where the ionization part was quite different in single-loss and -capture processes. It should also be pointed out that the intensities of C_{60}^{2+} ions in $1 \rightarrow 0$ and $1 \rightarrow 2$ spectra are much enhanced in comparison to the $2 \rightarrow 1$ spectra. In

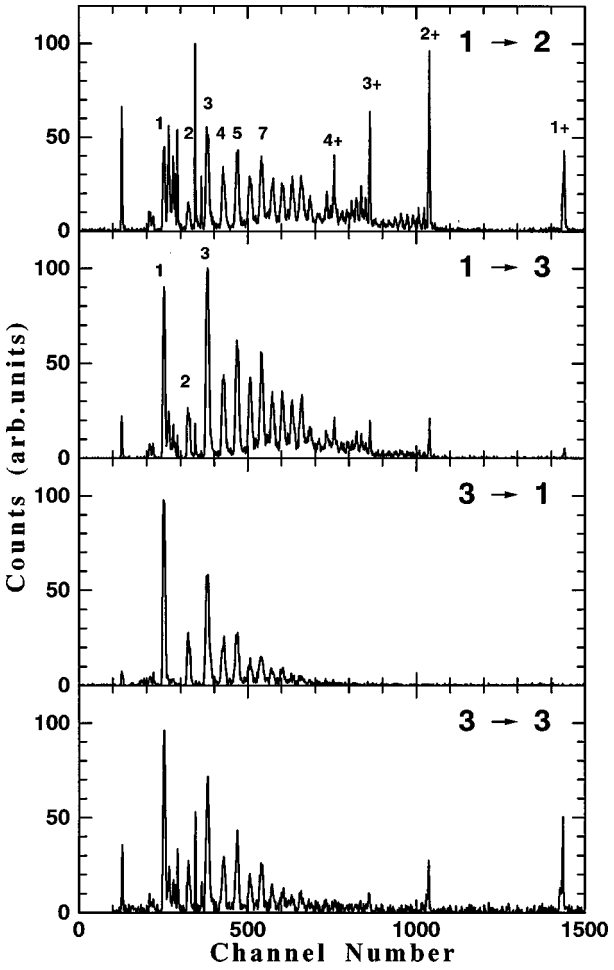

FIG. 5. Same as Fig. 4 but for Li^+ and Li^{3+} incidences.

the case of the double-loss process ($1\rightarrow3$), the ionization part decreases significantly compared to the single-loss process ($1\rightarrow2$) and a large enhancement is observed for $C_{1,3}{}^+$ ions compared to heavier fragment ions. All the spectra reveal a similar distribution pattern to the single-loss process of Li^{2+} projectiles ($2\rightarrow3$), indicating an equivalent influence on ionization and fragmentation of C_{60} in the two cases.

For Li^{3+} incidence, the spectral pattern was essentially equivalent in both processes of $3\rightarrow2$ and $3\rightarrow1$. In particular the ionization part nearly vanished compared to the fragmentation part and the intensity of C^+ was always larger than that of $C_3{}^+$ ions. Overall, the spectrum exhibits essentially the same pattern as the double-capture process of Li^{2+} ions. Similarly to the direct process of Li^{2+} ions, the ionization part is observed prominently in the $3\rightarrow3$ process. However, the fragmentation part is more strongly enhanced and the distribution pattern is close to that of other $3\rightarrow k$ processes.

B. Production cross sections

Absolute cross sections for fragmentation and ionization of C_{60} obtained for various charge-transfer processes are shown in Figs. 6(a)–6(c), where the cross sections for small fragment ions $C_n{}^+$ ($n=1-14$) and ionized parent ions $C_{60}{}^{r+}$ ($r=1-4$) are presented. Note that the values for $C_{60}{}^{4+}$ contain contributions from $C_{15}{}^+$ ions to some extent.

Some characteristics extracted from these data are given below. Most of the present cross sections are smaller than the geometrical C_{60} cross sections of $3.8\times10^{-15}\,cm^2$ (molecular radius 7 a.u.) and only some cross sections for Li^{3+} ions exceed this value. Apparently, the result implies that the collisions are taking place only within the molecular diameter. The oscillation of the cross sections is commonly observed for small fragment ions. The mass dependence of these cross sections is, however, significantly different for different incident charge states. For instance, the cross sections do not change very much for Li^+ ions but exhibit strongly a power-law-like behavior for Li^{3+} ions.

The direct process ($q\rightarrow q$) always gives the largest cross sections for the production of ionized parent ions. This is easily understandable because the ionization, which is often called pure ionization in ion-atom collisions, can take place in distant as well as close collisions. On the other hand, the electron capture and loss may occur only at relatively small impact parameters at the present incident velocity.

Surprisingly, the predominance of the direct process is also true for the production of small fragment ions for $q=1$ and 2 incidences, while the single-capture process is predominant for $q=3$ incidence. The result indicates strongly that the direct process induces high excitation of C_{60}, resulting in disintegration of the molecule with much higher probabilities than the charge-transfer processes.

It is noteworthy to compare the present data with charge-changing cross sections obtained for 2-MeV Li^{q+} ions in a gaseous material with atomic number equivalent to that of the carbon atom. The total production cross sections for $q\rightarrow k$ process obtained by summing over all relevant ions including large daughter ions $C_{60-2m}{}^{r+}$ are compared in Fig. 7 with previously reported charge-changing cross sections obtained for the N_2 target [35,36]. One can see a remarkable similarity between the two data apart from the relative magnitudes of the cross sections. In the present work, however, exact values of charge-changing cross sections cannot be derived since the background contribution is unknown.

C. Ionization and fragmentation

It is well known that the outstanding property of C_{60} in comparison to other usual molecules is its high stability against the Coulomb repulsive force [9,10,24]. This implies that the C_{60} molecule has an atomic property in the sense of ionization. It is therefore interesting to compare the cross sections for $C_{60}{}^{r+}$ ions with those obtained in ion-atom collisions of collision systems similar to those in the present work. This is demonstrated in Fig. 8, where the cross sections for Li^{3+} incidence are compared with those for 2-MeV $C^{3+}+Ar$ obtained using a similar experimental method [37]. Note that the incident velocity of carbon ions ($v=2.6$ a.u.) is slightly lower than the present lithium ions and also the total number of target electrons is significantly different in both cases. In spite of these differences one can see clearly the following. For the direct process ($3\rightarrow3$) the ionization cross sections seem to behave similarly in both cases. Indeed, the average values of the degree of ionization obtained by $\overline{r}=\Sigma r\sigma(r)/\Sigma\sigma(r)$ are about the same for both cases: $\overline{r}=1.5$ (C_{60}) and 1.4 (Ar). However, a careful comparison shows that cross-section ratios between $C_{60}{}^{r+}$ and Ar^{r+} in-

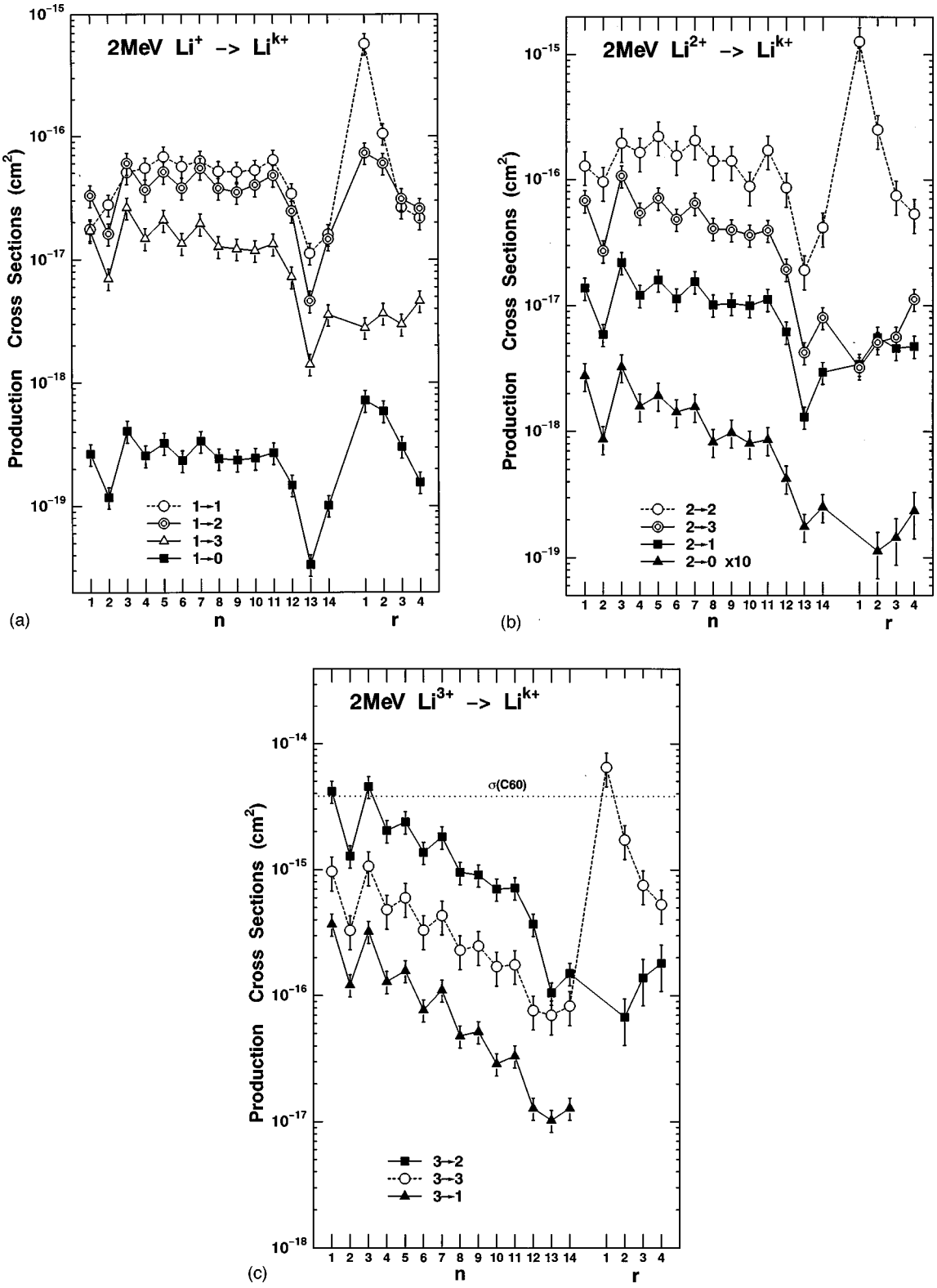

FIG. 6. Production cross sections of fragment ions C_n^+ and ionized parent ions C_{60}^{r+} measured for charge-transfer and direct collisions for (a) Li^+, (b) Li^{2+}, and (c) Li^{3+} ions. The abscissa represents the number of n and r.

crease from about 5 ($r=1$) to 10 ($r=4$). Qualitatively, outer-shell electrons are predominantly ionized and hence the ionization cross sections become large for smaller ionization potentials. The large enhancement of ionization cross sections observed at larger r can be understood easily since the ionization potential of the C_{60}^{r+} ion given by $7.59+3.82r$ (eV) [11,15] is substantially smaller than that of the Ar^{r+} ion for all r investigated here [38,39]. On the other hand, for the single-capture process ($3\rightarrow 2$) the cross sections increase with increasing r for C_{60}, while for the Ar target the maximum cross section is observed at $r=2$. We found that $\bar{r}=3.3$ for C_{60} is one unit higher than $\bar{r}=2.3$ for

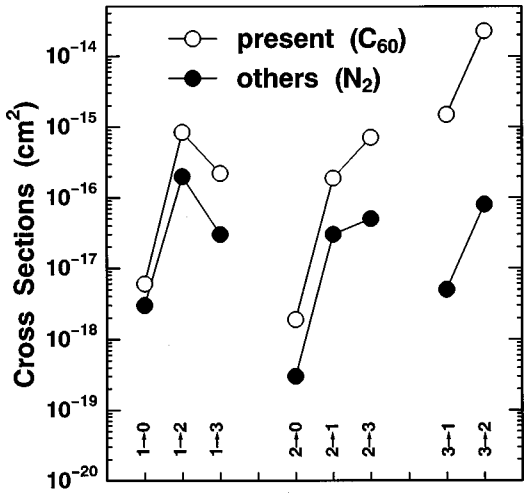

FIG. 7. Comparison between total production cross sections for the $q \rightarrow k$ process and charge-changing cross sections ($q \rightarrow k$) for 2-MeV $Li^{q+} + N_2$ [35,36]. The abscissa represents the collision processes $q \rightarrow k$.

the Ar target. This result seems to indicate that the bare Li^{3+} ions capture an electron preferentially from the 1*s* shell of a carbon atom to the projectile 1*s* shell, giving rise to one more ionization due to the Auger effect. The nearly absent C_{60}^{+} peak in the TOF spectra also supports this conclusion. This so-called *KK* electron transfer, which has already been observed in 15.6-MeV $C^{6+} + C_{60}$ collisions [27], is known to become important for fast bare ions provided the incident velocities are comparable to or higher than the target 1*s* electrons [40]. In the present case, the velocity of Li^{3+} ions is slower by only about 30% than that of C 1*s* electrons with a binding energy of 288 eV, so the transfer probability is supposed to be large. In contrast, in $C^{3+} + Ar$ collisions such an inner-shell transfer (from *L*-shell electrons in this case)

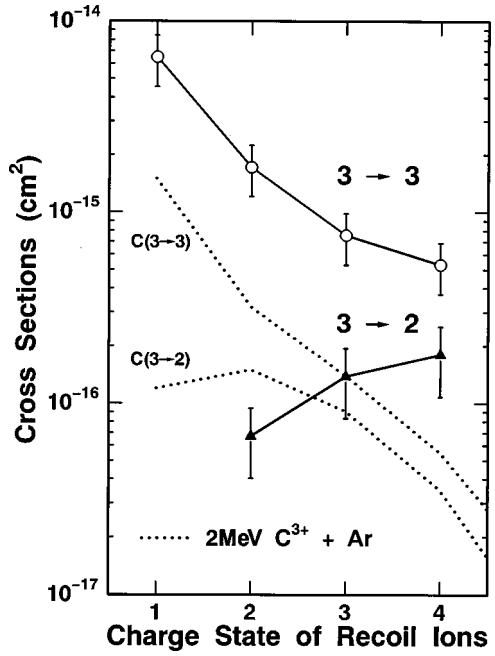

FIG. 8. Comparison of target ionization cross sections between $Li^{3+} + C_{60}$ and 2-MeV $C^{3+} + Ar$ collisions [37].

may be less probable because of the large energy difference between the electron binding energy of the initial and final states. A similar increase of multiply charged C_{60}^{r+} ions observed in $2 \rightarrow 0$ collisions [Fig. 6(b)] can also be partly interpreted by this *KK* electron transfer.

It is obvious that the energy *E* deposited on a target molecule from a projectile ion plays an important role in the fragmentation and ionization processes. For instance, it may be plausible to state that when *E* is small only ionization would occur and fragmentation would become important with increasing *E* [20]. As mentioned above, the distribution pattern differs significantly for different $q \rightarrow k$, indicating different *E* values for each process. Following a detailed report given by Cocke and Olson [41] on the mechanism of recoil ion production in ion-atom collisions, the total energy deposition *E* may consist of (a) the recoil ion energy, (b) the excitation energy of the recoil ion, (c) the sum of the ionization potentials required to produce a given recoil charge state, and (d) the kinetic energy of electrons either ejected into continuum states or captured by the projectile ions. In collisions between fast ions and the atomic target the first two components are small values in comparison to other components and can in general be discarded from the discussion [41,42]. In the present case of C_{60}, the argument about (a) may also be true because the kinetic energies of ionized parent ions are less than 0.1 eV. However, it is expected that the fragmentation of C_{60} is induced by a high degree of internal excitation among 240 valence electrons. As for the distribution of the total energy deposition *E* into components (a), (c), and (d), Olson, Ullrich, and Schmidt-Böcking [43] calculated using the *n*-body classical-trajectory Monte Carlo method for the collision system 1.4-MeV/nucleon $U^{32+} + Ne$. They determined each fractional energy as a function of the recoil ion charge state from 1 to 8. One can see in their paper that the fractions are roughly 50% for (d), 20% for (c), and less than 0.1% for (a). It is unfortunately impossible to determine these fractional energies from the present results. However, if we assume that the degree of ionization and the degree of fragmentation are both proportional to the total energy deposition, these two quantities should exhibit a positive correlation. Such a correlation between ionization and fragmentation was clearly observed in our case, as demonstrated in Fig. 9. Here we plot the average charge of recoil C_{60}^{r+} ions $\overline{r}$, defined above, as a function of the degree of fragmentation obtained by the ratio between the total cross sections S_{qk} of small fragment ions up to $n = 14$ and the sum of all cross sections shown in Fig. 7. Here we assume that large daughter ions C_{60-2m}^{r+} originate from the ionized parent ions [14,29] and these intensities were not included in the fragmentation intensity. A straight line crossing the origin of the coordinates can reproduce well these data within experimental errors, which provides clear evidence of the strong correlation between the two processes. Since the origin of the coordinates can be supposed as zero energy deposition, it is obvious that neither ionization nor fragmentation can occur at this point. It should be pointed out that the direct process always gives small values for both quantities. This is due to the large cross sections of the ionization part. The present result also supports the speculation that the pure ionization occurs at large impact parameters in which the energy deposition is small, so the average *E* value in direct pro-

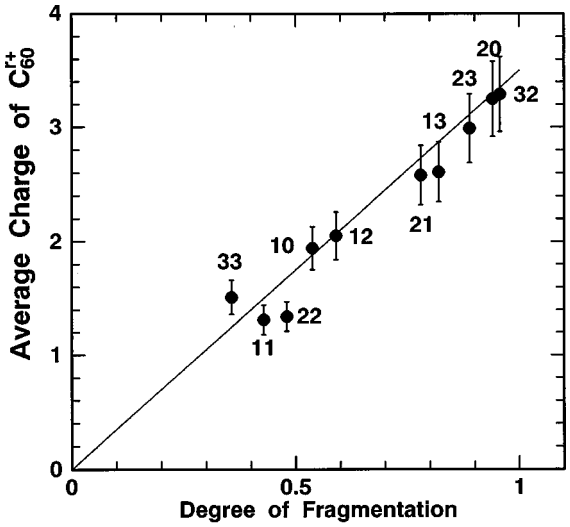

FIG. 9. Average charge $\bar{r}$ of C_{60}^{r+} ions as a function of the degree of fragmentation (see the text). Note that no parent ions are observed for the $3\rightarrow1$ process.

cesses becomes small compared to that in charge-transfer processes.

In order to see more clearly the ''degree of violence'' of collisions, the fractions of the first three small fragments (C_{1-3}^{+}) out of all the fragment ions (C_{1-14}^{+}) are plotted in Fig. 10 as a function of E estimated from [44] in the following way. For 2-MeV Li ions the TRIM program [44] gives stopping cross sections (eV cm^2) per carbon atom as $S_e = 6.13\times10^{-14}$ and $S_n = 8.25\times10^{-17}$ for electronic and nuclear stopping, respectively. The total energy deposition E was then calculated with the surface number density, $\rho = 60/4\pi a^2 = 3.9\times10^{15}\,(\mathrm{cm}^{-2})$ with $a = 7$ a.u. and by taking into account the two surfaces of the C_{60} cage, as $E(\mathrm{trim}) = 2\rho S_e = 478$ eV per molecule. The corresponding nuclear stopping energy was only 0.6 eV. It should be noted that the

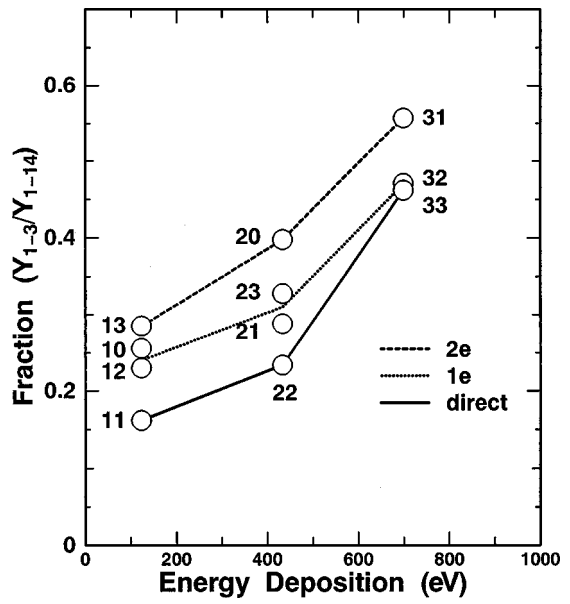

FIG. 10. Fraction of the first three small fragments out of the total small fragment ions Y_{1-3}/Y_{1-14} as a function of energy deposited on the target molecule (see the text).

TRIM calculation is made with an effective projectile charge Z_{eff}, which was estimated to be 2.48 for Li ions from the same calculation for hydrogen ions: $Z_{\mathrm{eff}}^2 = S_e(\mathrm{Li})/S_e(\mathrm{H})$. The energy deposition $E(q)$ for incident charge q was obtained from $E(q) = (q_{\mathrm{eff}}/Z_{\mathrm{eff}})^2 E(\mathrm{trim})$. The effective charges q_{eff} used for $q = 1$, 2, and 3 are, respectively, 1.26, 2.36, and 3 calculated by $n[I(q-1)/I(H)]^{1/2}$, where $I(q-1)$ is the ionization potential of $Li^{(q-1)+}$, n is the principal quantum number, and $I(H) = 13.6$ eV is for the hydrogen atom. The estimated E for Li^{q+} ions are 123, 433, and 700 eV for $q = 1$, 2, and 3, respectively. Figure 10 shows that overall the violent fragmentation becomes significant with increasing incident charge q as expected, and seems to saturate at small E values. Another remarkable feature extracted from this figure is that the degree of violence also increases with increasing number of electrons captured by or lost from the projectiles in collisions. Namely, in a fixed incident charge the largest values are obtained for two-electron-capture or -loss processes and the smallest values for direct processes. In electron-capture process the incident energy of the projectile is spent for the translational energy of the captured electron, 155 eV/electron in the present case, in addition to the total ionization potentials of the electrons. Therefore, relatively large E values are expected for capture collisions. The enhancement observed for double-capture processes may reflect this effect. As another interpretation we speculate that the two-electron processes may be induced preferentially by double collisions taking place at the front and the back surface of the C_{60} molecule. Such double collisions are supposed to have small probabilities compared to single-collision processes, resulting in smaller cross sections, as can be seen in Fig. 6. In turn, the total E value would increase substantially in double collisions, inducing more violent fragmentation.

D. Quasiequilibrium charge distribution

As discussed above, fragmentation of C_{60} is supposed to occur primarily when a projectile ion penetrates the molecular cage. In this situation the C_{60} molecule may act on the projectile as a thin carbon foil target with a thickness of 0.16 μg/cm^2. Thus the total cross sections summed over all small fragment ions in a given $q\rightarrow k$ process would provide useful information about the charge-state distribution (CSD) of outgoing projectiles after penetration through the cage. The CSD F_{qk} for the $q\rightarrow k$ process was calculated by $S_{qk}/\Sigma_{k=0}^{3} S_{qk}$, with S_{qk} defined above, and the results are presented in Fig. 11. Surprisingly, nearly the same CSD is obtained for Li^{2+} and Li^{3+} projectiles. For the Li^{+} incidence the distribution shifts to a lower side, but the magnitudes for $k = 1-3$ are comparable. The result indicates strongly that the penetrating projectiles can attain a nearly equilibrium charge distribution. Similar speculation about this equilibration was also pointed out by Walch *et al.* [21]. The average outgoing charge states $\Sigma_{k=0}^{3} k F_{qk}$ are estimated to be 1.7, 2.2, and 2.1 for Li^{+}, Li^{2+}, and Li^{3+}, respectively. The latter two values are comparable to the equilibrium mean charge 2.17 calculated from the semiempirical formula derived by Shima *et al.* [45] for energetic heavy ions in a carbon foil. Note that the effective charge ($Z_{\mathrm{eff}} = 2.48$) deduced from the TRIM calculation is an essentially different quantity from the

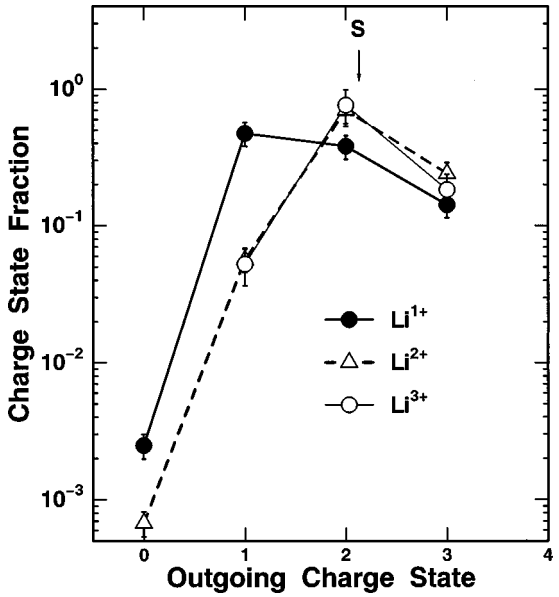

FIG. 11. Outgoing charge-state distribution obtained from the total production cross sections of small fragments for the individual $q \rightarrow k$ process ($k=0-3$). The letter *S* denotes the calculated equilibrium mean charge from [45]. Note the quasiequilibrium CSD.

equilibrium mean charge. At the present stage, no experimental data are available for the equilibrium charge of lithium ions in carbon foils at this projectile energy.

IV. CONCLUSIONS

Experimental results are reported for the production of carbon cluster ions from C_{60} molecules bombarded by 2-MeV $Li^{1+,2+,3+}$ ions. Production cross sections of individual fragment ions and intact parent ions are presented for charge-transfer as well as direct collision processes. Most cross sections were substantially smaller than the geometrical C_{60} cross section, indicating apparently that the interactions between collision partners occur predominantly within the C_{60} cage. It should, however, be emphasized that the information about impact-parameter-dependent probabilities in charge-transfer and ionization collisions is required to gain clear insight into this speculation.

The TOF pattern of the mass-to-charge distribution was found to be significantly different for different incident charge. For a given incident charge, the distribution of small fragment ions seems to be more or less the same pattern irrespective of outgoing charge states, with a few exceptions such as the large enhancement of lighter fragments compared to heavier ones. Instead, the most striking feature observed for a given incident charge is the dramatic change of relative intensities between the fragmentation part and the ionization part. For instance, in the Li^{2+} incidence, the ionization part is intensive for $2 \rightarrow 1$ collisions but is almost invisible for $2 \rightarrow 0$ collisions compared to the fragmentation part. In contrast, the ionization part is always produced predominantly in the direct process $q \rightarrow q$ for all the incident charges.

The atomic property of the C_{60} molecule was demonstrated by investigating parent ion production in comparison with recoil ion data obtained in usual ion-atom collisions [37]. An indication of the preferential *KK* electron transfer in electron capture by Li^{3+} ions was found from the enhancement of multiply charged parent ions. This is probably the case also for the Li^{2+} ions.

We found a strong positive correlation between ionization and fragmentation (Fig. 9), namely, the larger the degree of ionization, the larger the degree of fragmentation. The results suggest that both the ionization and the fragmentation are proportional to the total amount of energy deposition. Furthermore, the degree of fragmentation is largely enhanced in two-electron-capture or -loss processes compared to direct and one-electron processes. The results indicate that the energy deposition is different for each collision process even for the same incident charge. We speculate that the two-electron processes occur via double collisions of the single-electron process at the front and the back surface of the C_{60} cage.

From the arguments given above, it can be concluded that the ionization part in direct processes is induced at relatively large impact parameters, while in charge-transfer processes it occurs within the size of the target molecule. Also, the fragmentation part observed in all the collision processes is supposed to be produced by the penetration of incident ions through the cage, giving rise to a large enough energy deposition to cause the C_{60} fragmentation. Indeed, the spectra for a given incident charge exhibit similar distribution patterns irrespective of outgoing charge states. Finally, a rather astonishing result concerning the outgoing CSD was obtained from the total production cross sections of small fragment ions (Fig. 11). A nearly equivalent CSD irrespective of the incident charge states is certainly evidence that the outgoing projectiles are quasiequilibrated after passing through the C_{60} cage with a thickness of only 0.16 $\mu g/cm^2$.

ACKNOWLEDGMENTS

We gratefully acknowledge Dr. G. Schiwietz at HMI-Berlin and Dr. Y. Nakai at RIKEN for their valuable suggestions on this work. We would also like to thank A. Yogo and S. Anada for their help during measurements and M. Imai, K. Yoshida, and K. Norizawa for their technical support during the experiment.

[1] H. Haberland, in *Clusters of Atoms and Molecules*, edited by J. Peter Toennies, Chemical Physics Vol. 52 (Springer, Berlin, 1994).

[2] R. K. Yoo, B. Ruscic, and J. Berkowitz, J. Chem. Phys. **96**, 911 (1992).

[3] J. W. Keller and M. A. Coplan, Chem. Phys. Lett. **22**, 89 (1992).

[4] I. V. Hertel, H. Steger, J. de Vries, B. Weisser, C. Menzel, B. Kamke, and W. Kamke, Phys. Rev. Lett. **68**, 784 (1992).

[5] T. Drewello, W. Krätschmer, M. Fieber-Erdmann, and A.

Ding, Int. J. Mass Spectrom. Ion Processes **124**, R1 (1993).
[6] R. Völpel, G. Hofmann, M. Steidl, M. Stenke, M. Schlapp, R. Trassl, and E. Salzborn, Phys. Rev. Lett. **71**, 3439 (1993).
[7] S. Aksela, E. Nõmmiste, J. Jauhiainen, E. Kukk, J. Karvonen, H. G. Berry, S. L. Sorensen, and H. Aksela, Phys. Rev. Lett. **75**, 2112 (1995).
[8] R. Wörgötter, B. Dünser, P. Scheier, and T. D. Märk, J. Chem. Phys. **101**, 8674 (1994).
[9] P. Scheier and T. D. Märk, Phys. Rev. Lett. **73**, 54 (1994).
[10] T. D. Märk and P. Scheier, Nucl. Instrum. Methods Phys. Res. B **98**, 469 (1995).
[11] H. Steger, J. Holzapfel, A. Hielscher, W. Kamke, and I. V. Hertel, Chem. Phys. Lett. **234**, 455 (1995).
[12] D. Muigg, P. Scheier, K. Becker, and T. D. Märk, J. Phys. B **29**, 5193 (1996).
[13] S. Matt, B. Dünser, M. Lezius, H. Deutsch, K. Becker, A. Stamatovic, P. Scheier, and T. D. Märk, J. Chem. Phys. **105**, 1880 (1996).
[14] M. Foltin, O. Echt, P. Scheier, B. Dünser, R. Wörgötter, D. Muigg, S. Matt, and T. D. Märk, J. Chem. Phys. **107**, 6246 (1997).
[15] S. Matt, O. Ech, R. Wörgötter, V. Grill, P. Scheier, C. Lifshitz, and T. D. Märk, Chem. Phys. Lett. **264**, 149 (1997).
[16] A. Itoh, H. Tshuchida, K. Miyabe, T. Majima, and N. Imanishi, J. Phys. B. **32**, 277 (1999).
[17] P. Hvelplund, L. H. Andersen, H. K. Haugen, J. Lindhard, D. C. Lorents, R. Malhotra, and R. Ruoff, Phys. Rev. Lett. **69**, 1915 (1992).
[18] H. Shen, P. Hvelplund, D. Mathur, A. Bárány, H. Cederquist, N. Selberg, and D. C. Lorents, Phys. Rev. A **52**, 3847 (1995).
[19] R. Ehlich, M. Westerburf, and E. E. B. Campbell, J. Chem. Phys. **104**, 1900 (1996).
[20] E. E. B. Campbell, T. Raz, and R. D. Levine, Chem. Phys. Lett. **253**, 261 (1996).
[21] B. Walch, C. L. Cocke, R. Voelpel, and E. Salzborn, Phys. Rev. Lett. **72**, 1439 (1994).
[22] T. LeBrun, H. G. Berry, S. Cheng, R. W. Dunford, H. Esbensen, D. S. Gemmell, E. P. Kanter, and W. Bauer, Phys. Rev. Lett. **72**, 3965 (1994).
[23] S. Cheng, H. G. Berry, R. W. Dunford, H. Esbensen, D. S. Gemmell, E. P. Kanter, T. LeBrun, and W. Bauer, Phys. Rev. A **54**, 3182 (1996).
[24] J. Jin, H. Khemliche, H. Prior, and Z. Xie, Phys. Rev. A **53**, 615 (1996).
[25] J.-P. Briand, L. de Billy, J. Jin, H. Khemliche, M. H. Prior, Z. Xie, M. Nectoux, and D. H. Schneider, Phys. Rev. A **53**, R2925 (1996).
[26] A. Itoh, H. Tsuchida, K. Miyabe, M. Imai, and N. Imanishi, Nucl. Instrum. Methods Phys. Res. B **129**, 363 (1997).
[27] Y. Nakai, A. Itoh, T. Kambara, Y. Bitoh, and Y. Awaya, J. Phys. B **30**, 3049 (1997).
[28] T. Schlathölter, R. Hoekstra, and R. Morgenstern, J. Phys. B **31**, 1321 (1998).
[29] S. Martin, L. Chen, A. Denis, and J. Désesquelles, Phys. Rev. A **57**, 4518 (1998).
[30] H. Tshuchida, A. Itoh, Y. Nakai, K. Miyabe, and N. Imanishi, J. Phys. B **31**, 5383 (1998).
[31] W. C. Wiley and I. H. McLaren, Rev. Sci. Instrum. **26**, 1150 (1955).
[32] J. Abrefah, D. R. Olander, M. Balooch, and W. J. Siekhaus, Appl. Phys. Lett. **60**, 1313 (1992).
[33] C. K. Mathews, M. Sai Baba, T. S. Lakshmi Narasimhan, R. Balasubramanian, N. Sivaraman, T. G. Srinivasan, and P. Vasudeva Rao, J. Phys. Chem. **96**, 3566 (1992).
[34] V. Piacente, G. Gigli, P. Scardala, A. Giustini, and D. Ferro, J. Phys. Chem. **99**, 14 052 (1995).
[35] L. I. Pivovar, Yu. Z. Levchenko, and G. A. Krivonosov, Zh. Eksp. Teor. Fiz. [Sov. Phys. JETP **32**, 11 (1971)].
[36] V. S. Nikolaev, L. N. Fateeva, I. S. Dmitriev, and Ya. A. Teplova, Zh. Eksp. Teor. Fiz. [Sov. Phys. JETP **14**, 67 (1962)].
[37] M. Saito, Y. Haruyama, N. Hamamoto, K. Yoshida, A. Itoh, and N. Imanishi, J. Phys. B **28**, 5117 (1995).
[38] *CRC Handbook of Chemistry and Physics*, 67th ed. (CRC, Boca Raton, FL, 1987).
[39] W. Lotz, J. Opt. Soc. Am. **58**, 915 (1968).
[40] E. W. McDaniel, J. B. A. Mitchell, and M. E. Rudd, *Atomic Collisions, Heavy Particle Projectiles* (Wiley, New York, 1993).
[41] C. L. Cocke and R. E. Olson, Phys. Rep. **205**, 153 (1994).
[42] R. Schuch, H. Schöne, P. D. Miller, H. F. Krause, P. F. Dittner, S. Datz, and R. E. Olson, Phys. Rev. Lett. **60**, 925 (1988).
[43] R. E. Olson, J. Ullrich, and H. Schmidt-Böcking, Phys. Rev. A **39**, 5572 (1989).
[44] J. F. Ziegler, J. P. Biersack, and U. Littmark, *The Stopping and Range of Ions in Solids* (Pergamon, New York, 1985).
[45] K. Shima, T. Ishihara, and T. Mikumo, Nucl. Instrum. Methods **200**, 605 (1982); K. Shima, N. Kuno, M. Yamanouchi, and H. Tawara, At. Data Nucl. Data Tables **51**, 173 (1992).